Doi: 10.31276/VJSTE.61(4).09-13

New insights into the formation of amorphous molybdenum sulfide from a tetrathiomolybdate precursor

Anh D. Nguyen[1, 2*], Phuong T. Pham[2], An T. Dam[2], Phong D. Tran[2*]

[1]*Graduate University of Science and Technology, Vietnam Academy of Science and Technology*
[2]*University of Science and Technology of Hanoi, Vietnam Academy of Science and Technology*

Received 30 August 2019; accepted 7 November 2019

Abstract:

Amorphous molybdenum sulfide (MoS_x) is an attractive Pt-free catalyst for the hydrogen evolution reaction (HER) in both neutral and acidic pH electrolytes. Among the available approaches for the preparation of MoS_x, the electrochemical oxidation and reduction of a tetrathiomolybdate salt ($[MoS_4]^{2-}$) represents the most convenient. Herein we describe new insights onto the electrochemical oxidation of $[MoS_4]^{2-}$ to grow MoS_x thin films by employing an advanced technique called electrochemical quartz crystal microbalance (EQCM). These new findings enrich the current understanding of the structure, growth mechanism, redox property and catalytic operation of the MoS_x material.

One sentence summary: a new mechanism for growth of amorphous molybdenum sulfide thin films via the electrochemical polymerization of $[MoS_4]^{2-}$ is discussed.

Keywords: **EQCM, MoS_x formation, $[MoS_4]^{2-}$, $[Mo_3S_{11}]$ building block.**

Classification number: **2.1**

Introduction

Amorphous molybdenum sulfide, usually denoted as MoS_x, represents one of the most promising catalysts under investigation as the replacement for the Pt catalyst in the hydrogen evolution reaction (HER) of water. It shows excellent catalytic activity in both acidic and neutral pH electrolytes [1]. Its preparation can be achieved by different approaches like reactive magnetron sputtering [2], acidification of a $[MoS_4]^{2-}$ solution, electrochemical oxidation or electrochemical reduction of a deposition solution composed of $[MoS_4]^{2-}$ [3, 4], $[Mo_2S_{12}]^{2-}$ [5], or $[Mo_3S_{13}]^{2-}$ [5, 6]. In our previous work, we have demonstrated that MoS_x is a coordination polymer made of discrete $[Mo_3S_{13}]^{2-}$ building block clusters [4]. In the ideal circumstance where no structural defects like Mo-□ site are present within the polymeric structure of MoS_x, it could be described as a $(Mo_3S_{11})_n$ polymer. Treating MoS_x thin films or nanoparticles in an alkaline solution causes depolymerization that generates $[Mo_3S_{13}]^{2-}$ clusters that could be easily isolated, *e.g.* by adding Et_4N^+ cation [4]. Inversely, we recently demonstrated that electrochemical oxidation of the $[Mo_3S_{13}]^{2-}$ cluster *via* a two-electron process generated the MoS_x material [6]. A key elemental step was proposed to be the electrochemical elimination of the terminal disulfide ligand within the $[Mo_3S_{13}]^{2-}$ as the source of Mo-□ defects that subsequently served as anchoring sites for other $[Mo_3S_{13}]^{2-}$ clusters, thus driving polymerization. This means that during the growth of MoS_x materials, the $[Mo_3S_7]$ core skeleton is conserved.

$$[MoS_4]^{2-} \rightarrow MoS_3 + 1/8\ S_8 + 2e^- \qquad (eq.\ 1)$$

We then aim to revisit the polymerization of $[MoS_4]^{2-}$, namely a mononuclear species, into MoS_x which is made of $[Mo_3S_{13}]^{2-}$ building blocks. We note that the first discussion of the $[MoS_4]^{2-}$ to MoS_x polymerization mechanism was reported by Hu and co-workers [3, 7]. In that work, a rather simple reaction (*eq. 1*) was proposed based on the establishment of a relationship between the mass loss of the $[MoS_4]^{2-}$ precursor and the net charge consumed during the oxidation process. Furthermore, the amorphous molybdenum sulfide was described as MoS_3 which was not appropriate, as recent analysis has revealed the S: Mo atomic ratio within MoS_x should be closer to 4.0, e.g. ca. 3.7, rather than to 3.0 [4, 8]. We hypothesize the actual mechanism could be much more complicated than what has been described. In any case, the fundamental question of how the $[MoS_4]^{2-}$ mononuclear species can assemble into a

* *Corresponding authors: Email: nguyen-duc.anh@usth.edu.vn; tran-dinh.phong@usth.edu.vn*

$[Mo_3S_7]$ cluster within the MoS_x structure remains unclear.

Herein, employing an Electrochemical Quartz Crystal Microbalance (EQCM) analysis we show that the electrochemical oxidation of $[MoS_4]^{2-}$ precursor into MoS_x thin film occurs *via* a 10-electron process. Spectroscopic analyses clearly confirm the creation of the $[Mo_3S_{13}]^{2-}$ building block within MoS_x. A mechanism describing how $[MoS_4]^{2-}$ fragments assemble into the $(Mo_3S_{11})_n$ polymer, namely the MoS_x, is discussed.

Materials and methods

Materials

Ammonium tetrathiomolybdate ($(NH_4)_2[MoS_4]$) 99% and fluorine-doped tin oxide (FTO) coated glass were purchased from Sigma-Aldrich while Sulfuric acid (H_2SO_4), K_2HPO_4, KH_2PO_4, $K_3[Fe(CN)_6]$ and $K_4[Fe(CN)_6]$ were purchased from Xilong (99% purity). These chemicals were used as received without any further purification.

Electrochemical deposition and analyses

Electrochemical deposition and measurements were performed using a Biologic SP-50 potentiostat in a conventional three-electrode system. The working electrode was made of an FTO substrate for deposition of the MoS_x film which was then used for morphology and chemical composition characterization. For electrode mass change analysis, a AT-cut 5 MHz Au/Ti quartz QCM (S 1.31 cm^2) working electrode was used. A Pt plate was used as the counter electrode whereas the reference electrode was an Ag/AgCl (1 M KCl) electrode. All the potentials were reported on a normal hydrogen electrode (NHE).

The electrolyte solution consisted of 1 mM $(NH_4)_2[MoS_4]$ in a pH 7 phosphate buffer solution. Prior to use, the solution was filtered to remove any precipitates and then degassed by an N_2 flux for 30 min.

Cyclic voltammograms were recorded on the Au QCM electrode immersed in the electrolyte solution. The potential was polarized from 0 V towards 1.4 V then backwards to -1 V vs. NHE with a potential scan rate of 5 mV/s. The deposition of MoS_x was conducted using the chronoamperometric technique wherein the Au QCM electrodes were held at 0.33, 0.36 or 0.41 V vs. NHE. The total amount of charge passed through the working electrode for the MoS_x deposition was set at 10 mC/cm^2.

Bulk electrolysis

The number of electrons used per cluster during the oxidative deposition was determined using bulk electrolysis (chronoamperometric technique as aforementioned). During the electrolysis, the evolution of electrode mass was recorded. Because of the high sensitivity of QCM, a potential (e.g. 0.33 V) was only applied to deposit amorphous MoS_x on the electrode when the recorded mass was stable. We define a stable mass as changes less than 10^{-2} $\mu g/cm^2$ or lower. The deposition time was set for 500 s per cycle. The mass change was recorded in several repeated cycles.

Spectroscopic and microscopic characterization

The surface morphology of the MoS_x thin film was characterized by using a field emission scanning electron microscopy (FE-SEM, Hitachi S4800, Japan). Raman spectra were collected using a LabRAM HR Evolution Raman Microscope (Horiba) with the 532 nm green laser excitation. XPS analysis was conducted on a ULVAC PHI 500 (Versa Probe II) equipped with a monochromatic Al Kα (1486.6 eV) X-ray source.

Results and discussion

Electrochemical property of a $[MoS_4]^{2-}$ solution

We first re-investigated the electrochemical property of the $[MoS_4]^{2-}$ from the perspective of identification of suitable conditions for the electrochemical polymerization effect that generates MoS_x. Fig. 1 shows the first three consecutive cyclic voltammograms recorded on a clean FTO electrode immersed in a 1.0 mM $[MoS_4]^{2-}$ solution in pH 7 phosphate buffer. The potential polarization direction was set from the open circuit voltage towards the anodic potential with a potential scan rate of 50 mV/s. In the first cycle, two oxidation events are observed at potentials of 0 V and 0.95 V, while a reduction event is observed at -0.8 V vs. NHE (Fig. 1, blue trace). In the second and subsequent scans, the 0 V oxidation and the -0.8 V reduction events are unchanged. However, the 0.95 V oxidation event is no longer observable, and a new oxidation event at 0.41 V emerges (Fig. 1, red and green traces). Thus, to investigate the electrochemical polymerization of $[MoS_4]^{2-}$, we chose three potentials for chronoamperometry (CA) deposition, namely 0.33, 0.36 and 0.41 V vs. NHE, which corresponds to the foot-wave potential, half-wave potential and the peak potential of the latter oxidation event, respectively.

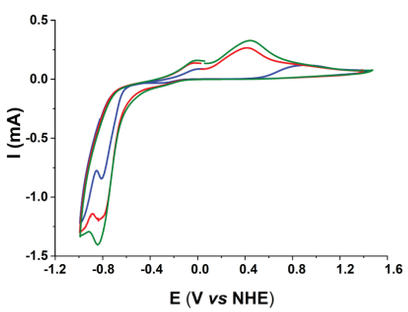

Fig. 1. Subsequent cyclic voltammograms (1st scan: blue trace; 2nd scan: red trace and 3rd scan: green trace) recorded on an FTO electrode immersed in a 1.0 mM $(NH_4)_2[MoS_4]$ solution in pH 7 phosphate buffer. The potential scan rate was 5 mV/s towards the anodic scan direction.

Characterization of deposited MoS_x films

In the same 1.0 mM $[MoS_4]^{2-}$ solution in pH 7 phosphate buffer, a clean FTO electrode was held at 0.33, 0.36 or 0.41 V vs. NHE for 2 hours to deposit brown-coloured MoS_x thin films.

Figure 2 shows the SEM images of these films. It can be seen that the obtained MoS_x films consist of clumps arranged close together in different shapes and sizes. The variation in clump shape and size are likely due to the different in the grown rate of MoS_x at different applied potential. There is no difference of morphologies observed between films prepared at various anodic potentials.

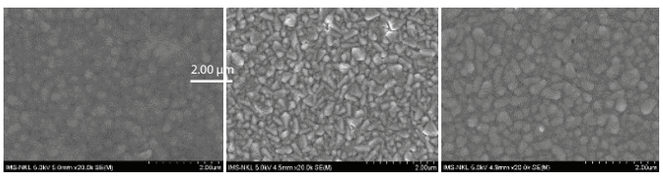

(A) (B) (C)

Fig. 2. SEM images of MoS_x grown at 0.33 (A), 0.36 (B), and 0.41 V vs. NHE (C).

Raman spectra clearly show all the characteristic features of a MoS_x polymeric thin film with $[Mo_3S_{13}]^{2-}$ building block clusters, as previously reported (Fig. 3) [4]. Vibrations at 284-382 cm^{-1} are assigned to the Mo-S bond, whereas the one at 450 cm^{-1} is attributed to the νMo_3-S_{apical} vibration mode. Vibrations of bridged or shared disulfide $(S\text{-}S)_{br/sh}$ and terminal disulfide $(S\text{-}S)_t$ are observed at 555 and 525 cm^{-1}, respectively.

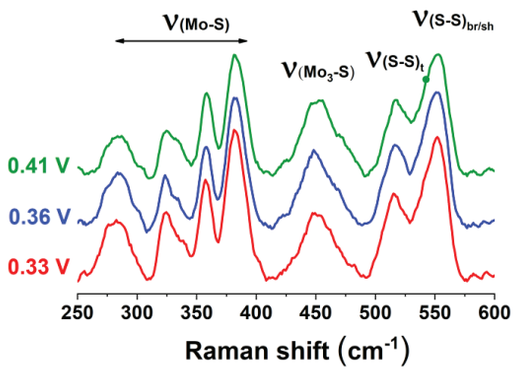

Fig. 3. Raman spectra recorded on the MoS_x films grown on FTO electrode at: 0.33 V (red trace), 0.36 V (blue trace), and 0.41 V vs. NHE (green trace).

In XPS analysis, Mo^{IV} species is characterized by a doublet having $Mo3d_{5/2}$ of 229.38 eV. The doublet at higher binding energy, $Mo3d_{5/2}$ of 230.30 eV, is attributed to Mo^{V} species, *e.g.* due to the presence of Mo^{V}=O defects. The presence of some Mo^{VI} species, like excess $[MoS_4]^{2-}$ or MoO_3, within the deposit is also likely as a doublet having $Mo3d_{5/2}$ of 232.44 eV is observed. The $(S\text{-}S)_{br/sh}$ disulfide ligand and the apical sulfide are characterized by a doublet having $S2p_{3/2}$ of 163.18 eV. While the doublet at $S2p_{3/2}$ of 162.07 eV is assigned to the terminal $(S\text{-}S)_t$ disulfide ligand (Fig. 4). The binding energies of Mo and S from XPS results are in consensus with the reported literatures [4, 6] and proving the obtained materials is amorphous molybdenum sulfide, labeled as MoS_x.

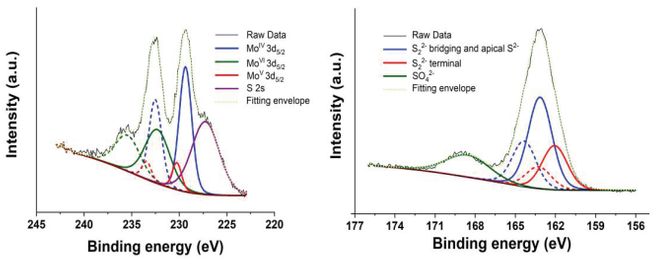

(A) (B)

Fig. 4. (A) Mo- and (B) S- core levels of a MoS_x film grown at 0.36 V vs. NHE. Similar features were recorded for the films grown at 0.33 V and 0.41 V.

These results confirm that at the potentials applied, $[MoS_4]^{2-}$ is electrochemically oxidized, which grows the MoS_x thin film consisting of $[Mo_3S_{13}]^{2-}$ building block clusters. In following section, we employ EQCM analysis to identify the number of electrons involved in each elemental electrochemical oxidation event.

Electrochemical quartz crystal microbalance analysis

A clean Au QCM electrode was first equilibrated in a 1.0 mM $[MoS_4]^{2-}$ solution in a pH 7 phosphate buffer for 30 minutes at the open circuit voltage. Subsequently, an anodic potential of 0.33 V vs. NHE is applied for a period of 500 s. We observed a linear increment of the electrode mass (Fig. 5A) that indicated growth, by electrodeposition, of material on the Au QCM electrode surface. When the applied potential was removed, no mass increment was recorded. This clearly confirmed that the MoS_x deposition is solely driven by the applied oxidation potential. From the mass increment we are able to deduce the amount of MoS_x deposited in moles under the assumption that the MoS_x is a perfect $(Mo_3S_{11})_n$ polymer without any structural defects or impurities. At the same time, the amount of charge involved in the process was recorded. We then plot the number of electrons (in mol) against the amount of Mo_3S_{11} clusters deposited (Fig. 5B). A slope of 9.65 is found. The same value was determined when we repeated the same deposition-relaxation process on the same electrode for several cycles (Figs. 5C, D).

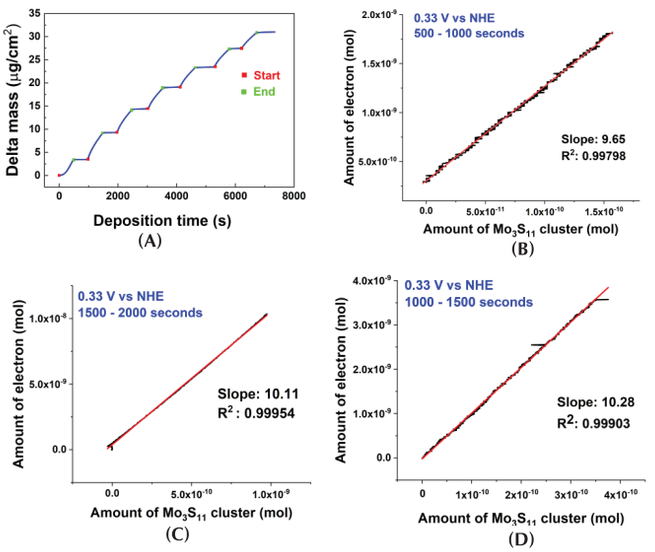

Fig. 5. EQCM analysis conducted on an Au QCM electrode held in a 1 mM $[MoS_4]^{2-}$ solution at 0.33 V vs. NHE. (**A**) evolution of the mass of the electrode as function of deposition time; (**B**, **C**, **D**) plots the electrode mass increment against the amount of electrons involved for different deposition periods.

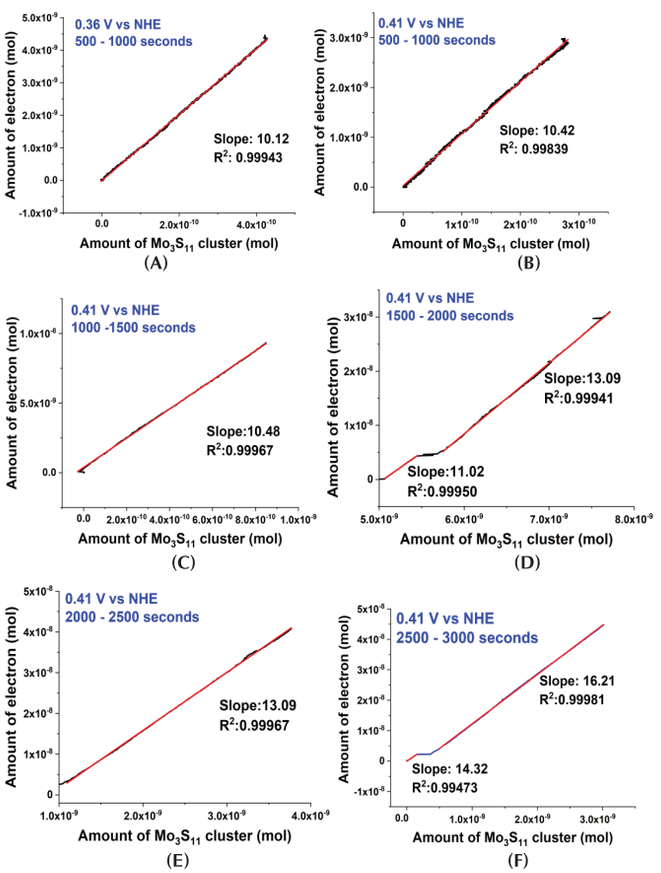

Fig. 6. Plot of electrode mass against the amount of electrons involved. (**A**) MoS_x film grown at 0.36 V and (**B**) 0.41 V vs NHE for a deposition period of 500-1,000 s. (**C**, **D**, **E**, **F**) MoS_x film grown at 0.41 V vs NHE for longer deposition periods.

At a higher applied potential, namely 0.36 V and 0.41 V vs. NHE, we observed the same phenomenon and a similar value of ca. 10 electrons over a (Mo_3S_{11}) cluster was determined (Figs. 6A, B). When the deposited film got thicker, e.g. after longer deposition time, the number of electrons involved was higher to generate the same (Mo_3S_{11}) cluster (Figs. 6C-F). This observation can be explained by the fact that MoS_x is not a good conductor. Thus, a thick layer of MoS_x may inhibit the electron transfer process. A similar phenomenon was also observed for the case of MoS_x films grown via an electrochemical oxidation of $[Mo_3S_{13}]^{2-}$ clusters [6].

Thus, based on the available data, we conclude that the MoS_x thin film is grown from the $[MoS_4]^{2-}$ solution via a 10-electron oxidation process during the early stages of deposition when the MoS_x film is not too thick. In other words, each Mo_3S_{11} unit comprising the MoS_x film is created *via* a 10-electron oxidation. This result is different compared with that reported by Hu, et al. [3, 7] where a 2-electron oxidation process was proposed (*eq. 1*) [3, 7]. The 10-electron oxidation process is given below:

$$3[MoS_4]^{2-} \rightarrow Mo_3S_{11} + 1/8S_8 + 10\ e^- \qquad (eq.\ 2)$$

Proposed mechanism for the growth of MoS_x film

We propose a mechanism for the growth of the $(Mo_3S_{11})_n$ polymer, namely the MoS_x film, *via* the electrochemical oxidation of $[MoS_4]^{2-}$. Our primary focus is on the mechanism behind the construction of a $[Mo_3S_{11}]$ skeleton by assembling three $[MoS_4]^{2-}$ fragment species through a 10-electron oxidation process. Firstly, a $[MoS_4]^{2-}$ molecule adsorbs to the electrode surface and loses 1 electron to create a Au-S covalent bond (Fig. 7A). Two other $[MoS_4]^{2-}$ molecules approach (Fig. 7B) and remove 6 electrons, which create three $(S\text{-}S)^{2-}$ ligands as well as a $Mo_3\text{-}S_{apical}$ mode (Fig. 7C). Actually, each $(S\text{-}S)^{2-}$ is generated from two S^{2-} ligands *via* a two-electron reaction:

$$2S^{2-} \rightarrow (S\text{-}S)^{2-} + 2e^- \qquad (eq.\ 3)$$

$$Mo^{VI} + 2e^- \rightarrow Mo^{IV} \qquad (eq.\ 4)$$

Here, the $[Mo_3S_7]$ skeleton grafted onto the electrode surface via a sulfide covalent bond is readily (Fig. 7D). In this $[Mo_3S_7]$ species, two Mo atoms are bound to two terminal S^{2-} ligands. These S^{2-} ligands could also be oxidized *via* a two-electron reaction, creating the terminal $(S\text{-}S)^{2-}$ ligand. This oxidation can also occur in parallel with the reduction of Mo^{VI} into Mo^{IV} (*eq. 4*). Alternatively, a S^{2-} ligand is oxidized by a two-electron process producing elemental sulfur and leaving a coordination vacancy on the Mo atom (Fig. 7E). Indeed, the presence of an elemental sulfur impurity in the MoS_x film has been discussed elsewhere [9, 10]. This vacancy then acts as an anchoring position to host a new $[MoS_4]^{2-}$ molecule. At this step, a

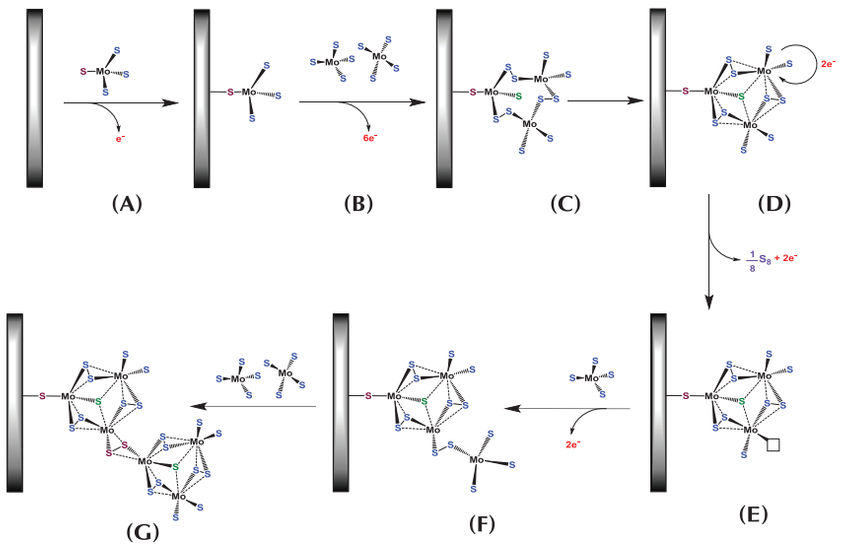

Fig. 7. Proposed mechanism of electro-oxidation synthesis of a-MoS_x from $[MoS_4]^{2-}$ precursor.

new $(S\text{-}S)^{2-}$ ligand is generated after removing two more electrons (Fig. 7F). The newly $[MoS_4]^-$ species grafted on the $[Mo_3S_7]$ cluster now continues its reaction in the same manner as the $[MoS_4]^-$ grafted on the Au electrode described above (Fig. 7G). Through such a reaction sequence, the $(Mo_3S_{11})_n$ polymer is grown on the Au electrode surface via a 10-electron oxidation process as determined experimentally in this work.

Conclusions

To conclude, the electrochemical oxidation of a $[MoS_4]^{2-}$ solution in neutral pH can grow an amorphous molybdenum sulfide (MoS_x) thin film, which is constructed of $[Mo_3S_{13}]^{2-}$ building blocks. Employing an electrochemical quartz crystal microbalance (EQCM) analysis, we revealed that the $[MoS_4]^{2-}$ molecule goes through a 10-electron oxidation process to create the (Mo_3S_{11}) structure unit and subsequently the $(Mo_3S_{11})_n$ polymer. A mechanism has been proposed to describe the elemental steps of such a 10-electron oxidation process. This work enriches the current knowledge of the formation, structure, and attractive redox property of the MoS_x.

ACKNOWLEDGEMENTS

This work is supported by Graduated University of Science and Technology (GUST - VAST) via project GUST. STS.DT 2017 - HH11. We acknowledge Dr. Nguyen Thu Loan and Prof. Ung Thi Dieu Thuy (Institute of Materials Science - VAST) for experimental support.

The authors declare that there is no conflict of interest regarding the publication of this article.

REFERENCES

[1] D.E. López, Z. Lou, N.V. Rees (2019), "Benchmarking the activity, stability, and inherent electrochemistry of amorphous molybdenum sulfide for hydrogen production", *Adv. Energy Mater.*, **9**, 1802614, Doi: 10.1002/aenm.201802614.

[2] F. Xi, P. Bogdanoff, K. Harbauer, P. Plate, C. Höhn, J. Rappich, B. Wang, X. Han, R. van de Krol, S. Fiechter (2019), "Structural transformation identification of sputtered amorphous MoS_x as an efficient hydrogen-evolving catalyst during electrochemical activation", *ACS Catal.*, **93**, 2368, Doi: 10.1021/acscatal.8b04884.

[3] D. Merki, S. Fierro, H. Vrubel, X. Hu (2011), "Amorphous molybdenum sulfide films as catalysts for electrochemical hydrogen production in water", *Chemical Science*, **2(7)**, pp.1262-1267.

[4] Phong. D. Tran, T.V. Tran, M. Orio, S. Torelli, Q.D. Truong, K. Nayuki, Y. Sasaki, S.Y. Chiam, R. Yi, I. Honma, J. Barber, V. Artero (2016), "Coordination polymer structure and revisited hydrogen evolution catalytic mechanism for amorphous molybdenum sulfide", *Nature Materials*, **15**, pp.640-646.

[5] O. Mabayoje, Y. Liu, M. Wang, A. Shoola, A.M. Ebrahim, A.I. Frenkel, C.B. Mullins (2019), "Electrodeposition of MoS_x hydrogen evolution catalysts from sulfur-rich precursors", *ACS Appl. Mater. Interfaces*, **11(36)**, pp.32879-32886, Doi: 10.1021/acsami.9b07277.

[6] Tuan M. Duong, Anh D. Nguyen, Ly T. Le, Loan T. Nguyen, Phong D. Tran (2019), "Insights into the electrochemical polymerization of $[Mo_3S_{13}]^{2-}$ generating amorphous molybdenum sulfide", *Chem. Eur. J.*, **25(60)**, pp.13676-13682.

[7] H. Vrubel, X. Hu (2013), "Growth and activation of an amorphous molybdenum sulfide hydrogen evolving catalyst", *ACS Catalysis*, **3(9)**, pp.2002-2011.

[8] J.D. Benck, Z. Chen, L.Y. Kuritzky, A.J. Forman, T.F. Jaramillo (2012), "Amorphous molybdenum sulfide catalysts for electrochemical hydrogen production: insights into the origin of their catalytic activity", *ACS Catal.*, **2(9)**, pp.1916-1923.

[9] J. Tan. W. Yang, Y. Oh, H. Lee, J. Park, J. Moon (2018), "Controlled electrodeposition of photoelectrochemically active amorphous MoS_x Cocatalyst on Sb_2Se_3 photocathode", *ACS Appl. Mater. Interfaces*, **10(13)**, pp.10898-10908, Doi: 10.1021/acsami.8b00305.

[10] X.J. Chua, M. Pumera (2018), "Molybdenum sulfide electrocatalysis is dramatically influenced by solvents used for its dispersions", *ACS Omega*, **3(10)**, pp.14371-14379.